The Corrosion of Materials in Water Irradiated by
800 MeV Protons

R.S. Lillard, D.L. Pile[✝], D.P. Butt[*]
Materials Corrosion and Environmental Effects Lab
Materials Science and Technology Division, MST-6
Los Alamos National Laboratory
Los Alamos New Mexico 87545

Abstract

A method for measuring the real-time corrosion rates for Alloy 718, stainless steels 304L and 316L nuclear grade, aluminum alloys 5052 (Al5052) and 6061 (Al6061), copper (Cu), tantalum (Ta), and tungsten (W) in two separate water systems that were irradiated by 800 MeV protons is presented. The first water system was fabricated entirely of 304 SS, thoroughly cleaned before operation, and employed hydrogen water chemistry (HWC) to mitigate the formation of some radiolysis products. Over the course of that irradiation period the corrosion rates for 304L SS, 316L-NG SS, Alloy 718, and Ta were, less than 1.2×10^{-6} m/yr. For Al6061 and Al5052 the corrosion rates were on the order of 5.0×10^{-7} to 2.0×10^{-6} m/yr. The corrosion rate of W was relatively high, between 5.0×10^{-6} and 3.0×10^{-5} m/yr. The second water system was fabricated from copper piping and steel components, was not cleaned prior to operation, and employed no HWC. In comparison to the stainless steel system, the corrosion rates in the copper/steel system were 1-3 orders of magnitude higher. These results are discussed in terms of water radiolysis and water impurity levels.

[✝]Present address: Dept. of Materials Science, University of Virginia, Charlottesville, VA, 22903

[*]Present address: Ceramatec Inc., 2425 South 900 West, Salt Lake City, Utah, 84119

1. Background

1.1 Water radiolysis

Spallation neutron sources typically consist of a high energy (0.6 - 1.4 GeV) proton accelerator (linac / synchrotron) and a shielded cavity which contains the neutron source (or target). This target is a high atomic number metal, for example tungsten (W) or tantalum (Ta). High energy neutrons are produced when the proton beam leaves the high vacuum of the accelerator via a "window" and enters the cavity where it then strikes the target. To keep the target cool (and to moderate the energy of the neutrons which are produced) it is enclosed in a cooling loop which is generally constructed from stainless steel 304 (304 SS) and filled with deionized water. The interaction of high energy protons with water results in the breakdown of water molecules to form a myriad of stable and short lived species. Water radiolysis models for both fission reactors[1-3] and linear accelerators[4] predict that similar species are formed in both environments including: H_2, O_2, H_2O_2, OH, H, e^-_{aq}, HO_2, O_2^-, HO_2^-, OH^-, H^+. A list of some of the possible decomposition mechanisms for these species and their respective rate constants are presented in Table 1. As indicated by the reaction rate constants, the lifetime of many of these species is short, on the order of microseconds to nanoseconds. With the exception of hydrogen peroxide (H_2O_2), oxygen (O_2), and hydrogen (H) the steady state concentration of these short lived species is typically on the order of 10^{-10} to 10^{-8} Molar (M). Therefore, while these short lived species may be an important consideration in the corrosion mechanism at the proton beam / metal / solution interface, i.e. at the Helmholtz layer where the steady state concentration will be high while the beam is on, they will have little impact on materials "downstream" in the cooling water loop.

Radiolysis products such as H_2O_2 and O_2 are the species most likely to influence the corrosion reaction mechanism of materials downstream from the beam because their lifetimes are on the order of days or weeks and, they are oxidizing species[5]. At the open circuit potential (OCP), anodic and cathodic reactions on the metal surface occur at the same rate. As corrosion reactions are generally cathodically limited, an increase in the concentration of an oxidizing species increases the cathodic reaction rate and, correspondingly, increases the anodic (metal oxidation)

reaction(6). It has been shown that an increase in concentration of total oxidant due to water radiolysis results in an increase in the OCP of structural materials in the cooling loop, such as austenitic stainless steels, to a potential region which is associated with an increased risk for stress corrosion cracking (SCC). Therefore, it is anticipated that the unmitigated production of H_2O_2 in a spallation neutron cooling water loop will result in higher corrosion rates as compared to a system that attempts to control the concentration of total oxidant $(H_2O_2 + O_2)$ by the addition of a scavenger gas (such as H_2)(5). For example, H_2O_2 is formed when two OH radicals combine:

$$OH + OH \xrightarrow{k_1} H_2O_2 \quad k_1 = 4.5 \text{x} 10^9 \text{ sec}^{-1} \tag{1}$$
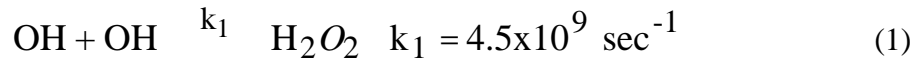
By bubbling H_2 gas into the system the OH radical preferentially reacts with the resultant dissolved atomic hydrogen in the cooling loop to form water:

$$OH + H \xrightarrow{k_2} H_2O \quad k_2 = 2.4 \text{x} 10^{10} \text{ sec}^{-1} \tag{2}$$
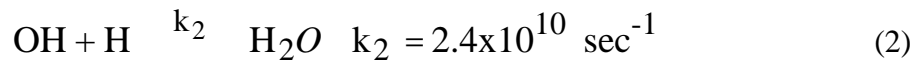
A similar reaction sequence can be written for O_2 formation and suppression. The ability of H_2 to suppress the concentration of total oxidant in a water system exposed to radiation has long been recognized by the boiling water reactor (BWR) community and is referred to as hydrogen water chemistry (HWC). To mitigate the increased susceptibility to SCC that results from high concentrations of total oxidant, a typical BWR operates at a dissolved hydrogen concentration on the order of 50 ppb. For BWRs as well as pressurized water reactors the OCP is greatly suppressed during HWC(7-13). The OCP can further be reduced by plating a small film (several 100 Å thick) of noble metal onto the interior surface of these components(14). These noble metals (such as Pd or Pt) have a high exchange current density for the reversible hydrogen reaction and in combination with HWC decrease the OCP to the potential for the reversible hydrogen reaction which is below the threshold potential for SCC.

1.2 Corrosion in irradiated water

Investigations of the effects of radiolyzed water on corrosion rate can be divided into two general categories: 1) simulated environments and 2) experiments where the electrochemical cell containing the working electrode (or weight loss coupon) is placed in either a Co^{60} or Ce^{137} source. In this latter category of experiments the OCP of stainless steels(15) and titanium(16) have been

observed to shift in the noble direction during irradiation. This positive increase in the OCP has been attributed to the radiolytic production of hydrogen peroxide, in a mechanism similar to that described above. However, by the nature of their set-up these experiments expose both the water and sample to -radiation and, therefore, do not separate the effect of radiolysis products from those effects associated with the direct -radiation of the sample. The direct exposure of metals to irradiation has been shown to effect both the defect structure and the conducting properties of the passive oxide, thus effecting metal dissolution rate and susceptibility to pitting(17, 18). For example, potentiodynamic polarization curves for Ti after 12 months exposure to brine solution with -radiation show small decreases in anodic current densities and limited thickening of the passive film as compared to unirradiated samples(19). X-ray photoelectron spectroscopy of the passive film on stainless steel after exposure to -radiation found that the surface oxide that was depleted in iron and enriched in chromium(20). Therefore, when investigating the effects of long-lived water radiolysis products on corrosion rate the effect of sample radiation must be eliminated. In this study, this was accomplished by separating the water manifold that allowed water to be circulated through the proton beam from the corrosion probes with adequate distance and shielding.

2. Experimental

2.1 The water systems

This paper reports the results from corrosion samples studied in two separate water systems. These systems shall be referred to as the "corrosion loop" and the "degrader loop" (Figure 1a and 1b respectively). Both systems were irradiated at the Los Alamos Neutron Science Center (LANSCE) A6 Target Station. Diagrams of this area may be found in earlier publications(21). The degrader loop was in operation during the late summer and early fall of 1995 while the corrosion loop was in operation during the spring and early summer of 1997. Each loop was attached to a water manifold that was directly exposed to 800 MeV protons during the course of the experiments. In the case of the degrader loop, the manifold consisted of a football

4

shaped baffle. Water flowing through this baffle had a residence time of approximately 16 seconds. In the case of the corrosion loop the water manifold held a set of the in-beam corrosion probes. Results from the in-beam probes address proton irradiation effects on corrosion and have been discussed in separate publications(22, 23).

The corrosion loop (Figure 1a)was a closed loop system, constructed entirely of 304 SS.[✢] While most all of the connections to this system were welded, threaded connections were sealed with reactor grade pipe dope. The nominal operating pressure was 1.03×10^6 Pa at a flow rate of 1 L/s. and a temperature of 20° C. Prior to placing the corrosion loop into operation it was steam cleaned. This was followed by several rinsings with a 50% DI water / 50% ethanol mixture. Finally, the system was rinsed several times with DI water. Each rinse entailed filling the expansion and reservoir tanks with the solution and circulating it through the system with the pump. In an attempt to mitigate the formation of hydrogen peroxide in the corrosion loop, HWC was employed. This was accomplished by bubbling a mixture of H_2 / 94% Ar gas directly into the water reservoir. The dissolved hydrogen concentration in the corrosion loop during the LANSCE irradiation experiments was monitored with a remote hydrogen sensor, Orbisphere Laboratories, Emerson NJ, (model #3610/220.E, TCD Hydrogen Gas System). Nominally, the system was operated with a dissolved hydrogen concentration of approximately 0.40 ppm. During some periods of irradiation the measured hydrogen concentration was greater than this value, presumably due to radiolytic hydrogen formation.

The degrader loop was also a closed loop system (Figure 1b). Although the water baffle and piping associated with the insert were constructed entirely of 304 SS, the piping associated with the pumping system and heat exchanger was constructed from copper as well as steel. Unlike the corrosion loop, no special cleaning of the system was employed before operation. Although the system was filled with deionized water, no HWC was employed. Nominally, the degrader loop operated at a pressure of 6.2×10^5 Pa, a flow rate of 0.32 L/s, and a temperature of approximately 30° C.

[✢] It is recognized that stainless steel 308 weld rods are used in the welding of 304 SS.

Both the corrosion and degrader water loops contained identical probes for measuring corrosion rate. These probes were located out-of-beam, downstream from the manifold and a considerable distance from any proton / neutron flux (designated as return and supply corrosion probes in Figures 1a and 1b). They were purchased off-the-shelf from a commercial vender. A diagram of the probe can be found in earlier publications(21). The probe consisted of a 304 SS NPT pipe plug style feed-through that supported 3 threaded studs. These studs were joined to the feed-through via a glass to metal seal that also provided electrical isolation. One end of the sample was tapped to accept the threaded stud on the feed-through. Electrical contact to the sample was via a coaxial cable and BNC connector on the feed-through. A water tight seal between the sample and glass was obtained via a Viton o-ring that was placed on each stud prior to screwing on the samples. The probes were fitted into "cells" constructed from 304 SS on both the supply and return sides of the cooling water loop at the top of the insert (approximately 3.4 m from the proton beam). These cells contained an inlet and outlet for the system water and held approximately 8 liters of water. A modified version of the three electrode out-of-beam corrosion probes was used to measure changes in water conductivity in both the corrosion and degrader loop. In the corrosion loop, the conductivity probes were constructed by welding a hollow 304 SS tube (approximately 7.5 cm long, 4 cm ID., and 0.15 cm wall) onto two of the threaded sample mounting studs of the NPT feed-through. This stainless steel sleeve surrounded a small 304 SS rod (6.4 cm long, 0.03 cm diam.) which was welded onto the third sample mounting stud. Because both ends of the sleeve were open and there was a separation distance of approximately 0.5 cm between the sleeve and the NPT probe, ample water flowed from one end of the sleeve to the other. To determine the cell constants of these probes, each probe was calibrated with solutions of known conductivity prior to placement in the system. One conductivity probe was placed in the supply stream and one in the return stream cells at the top of the inserts. Similar probes were used to measure conductivity in the degrader loop.

2.2. Proton beam characteristics

The proton beam characteristics at LANSCE have been describe in detail elsewhere(23, 24). Briefly, the proton beam flux at the LANSCE A6 Target Station had a Gaussian distribution of 2 3 cm. The energy of this particle beam was 800 MeV. The beam had a characteristic macropulse repetition rate of 100 Hz, a gate length of 835 microseconds, and a fixed peak current of 16 mA. Average proton beam currents were controlled by varying the spacing between each micropulse (and therefore the number of micropulses) in the gate. Nominally, the average proton beam currents varied between 0.001 and 1.0 mA. Calculated proton fluence as a function of irradiation time is presented in Figure 2(23). The measured fluence on both the degrader and corrosion manifolds at the end of the irradiation periods was on the order of 10^{20} p/cm^2. Although all experiments were conducted with the proton beam on (unless otherwise noted in the text), it should be re-emphasized that the out-of-beam samples reported on here where both up stream and down stream from the manifolds, well shielded from the proton beam and any secondary radiation.

2.3 Electrochemical

Corrosion samples were fabricated from rods approximately 0.318 cm in diameter by 5 cm to 7.6 cm in length. The samples placed in the corrosion loop were, Alloy 718 (UNS N07718, precipitation hardened, Cr-18 at%, Fe-19, Nb-5, Mo-3, Ni-53 min), aluminum alloys 6061 (UNS: A96061, T6 temper, referred to as Al6061) and 5052 (UNS A95052, T6 temper, referred to as Al5052), 304L SS (UNS S30403), 316L stainless steel nuclear grade(UNS S31653, referred to as 316L-NG SS), 99.8 % tungsten (W), and 99.95% tantalum (Ta). The samples placed in the degrader loop were Al6061, 304L SS, Alloy 718, and 99.99% copper (Cu). Prior to placing the corrosion samples on the probe, the surfaces were abraded with 600 grit SiC paper to expose a fresh metal/oxide surface for electrochemical characterization. The samples were then cleaned in an ultrasonic cleaner in successive baths of acetone, ethanol and DI water. The reference electrode was made by flame-oxidizing (in air) a tungsten sample(25). This reference electrode is referred to here as W/Wox. At pH 4.2, the pH of the water systems, the OCP of the W/Wox electrode was -0.045 V relative to saturated calomel (OCP$_{W/Wox}$=0.08-0.03pH; V vs. SCE). Because the OCP of

W/Wox electrode changed only 0.03 V / pH unit , corrections for small deviations in the water system pH were not needed. Further, the OCP of the W/Wox electrode was independent of hydrogen concentration as shown in Figure 3 and only slightly dependent on H_2O_2 concentration.

To measure the polarization resistance (R_{pol}) of each sample as a function various irradiation conditions, electrochemical impedance spectroscopy (EIS) was used. EIS is a powerful non-destructive technique for measuring the corrosion rates of metals in aqueous environments(26, 27) and is ideally suited for systems with high solution resistivity. Here a small sinusoidal voltage perturbation (30 mV) was applied across the sample interface over the frequency range of 0.003 Hz to 1.0 k Hz. By measuring the transfer function of the applied ac voltage perturbation and the ac current response of the sample, an impedance resulted ($Z = V / I$). In the simplest sense, at low frequencies the sample behaved as a resistor and the impedance was equal to the sum of the polarization and solution resistance ($Z_{lo} = (R_{sol} + R_{pol})$). At high frequencies, the sample behaved as a capacitor and, therefore, offered no resistance to the ac current and $Z_{hi} = R_{sol}$. By measuring Z over a wide frequency range, R_{pol} can be quantified by subtracting R_{sol} from Z_{lo}. All EIS experiments were conducted at the sample's open circuit potential (OCP; i.e., it's free corrosion potential). Data were collected in the traditional 3 electrode configuration where the W/Wox electrode served as a reference and three, electrically connected, alloy C276 samples served as the counter electrode. In addition, the EIS system used in this investigation operated with a floating ground to avoid interference from ground loops.

For the corrosion loop, initial irradiation experiments were conducted during proton irradiation at average proton beam currents of 0.001, 0.010, 0.04, 0.10, and 0.40 mA. That is, electrochemical measurements were conducted while the proton beam was on. These data were taken with all other inserts (17A - 18C in Figure 4) pulled out of the proton beam path such that the first material that the proton beam struck after leaving high vacuum was tube #1 of the corrosion manifold (17B). Thermocouples attached to the front of the manifold verified the position, size and shape of the proton beam. After approximately 300 hrs of experiments with only the corrosion insert in place, inserts 17A, 18A, 18B, and 18C were placed in position in front of the corrosion

insert and the beam current was increased to 1.0 mA. The effect of these inserts in front of the corrosion insert was to spread the proton beam from its compact Gaussian distribution to a more diffuse, cloud-like beam. That is, for any given current the beam flux at the corrosion loop insert was lower with the forward inserts in place.

For the degrader loop experiments, at no time were inserts placed between the uhv window and the water degrader manifold. Therefore, there is no reason expect that the beam flux deviated from the anticipated profile(24) during the course of the experiments.

3. Results and Discussion

3.1 OCP Measurements

For the materials that were the most active (least noble), some difference was observed between the OCP of the return side sample and the OCP of the supply side sample during irradiation. This is best illustrated in the OCP of the Cu samples in the degrader loop (Figure 5). When the beam was turned on, a sharp 0.075 V increase in the OCP of the return side sample from its steady state value was observed. In addition, when the beam was shut off, a sharp decrease in the OCP was also observed. No change in the OCP of the supply side probe from its steady state value was observed when the beam was turned on. In addition to the changes observed in the OCP of the return side samples, a gradual increase in the OCP of all samples (supply and return, degrader and corrosion loops) was observed over the course of both irradiation periods (Figure 6). This gradual increase in OCP with irradiation time is consistent with an increase in the concentration of total oxidant as discussed above.

3.2 CNLS modeling of EIS data and corrosion rate

Typical EIS data are presented in Figures 7a for Alloy 718 (corrosion loop) and Figure 7b for 304L SS (degrader loop). These figures are representative of the data for all samples in this study although the magnitude of the impedance was a function of sample material, sample location, and beam parameters . The equivalent circuits (EC) used to model these data are presented in Figures 8a and 8b. The EC in Figure 8a is referred to as a Simplified Randle's Circuit and was used when the response of the material was similar to that in Figure 7a. In this model, R_{pol}

9

represents the polarization resistance of the material, C_{dl} the double layer capacitance, and R_{sol} the geometric solution resistance between the working and reference electrodes. Typical curve fits of this model to the data are presented in Figure 7a as solid and dashed lines. As can be seen in this figure, good agreement between the model and the data exists. At longer immersion times a Warburg (diffusion) component in the EIS spectra of some samples was observed. This response was characterized by the change in the slope of the low frequency data from -1 to approximately -1/2 (at approximately 4.0 Hz in Figure 7b). For these data, the EC in Figure 8b was used where Z_W represents the diffusional (Warburg type impedance) and all other elements are as before. Once again, good agreement between the model and the experimental data exist as represented by the solid and dashed lines in Figure 7b.

From the CNLS values of R_{pol}, the corrosion rate of each sample was calculated as a function of immersion time. In these calculations i_{corr} was derived from R_{pol} by the Stern-Geary relationship(28):

$$i = 2.303 i_{corr} \frac{a + c}{a\ c} \left(E_{ap} - E_{corr}\right)$$ (3)

where: i is the applied current density, i_{corr} is the corrosion current density, E_{corr} is equal to the OCP, $_{ap}$ is the applied potential, $_a$ and $_c$ are the anodic and cathodic Tafel slopes. In this relationship $1/R_{pol}$ is equal to $i/(E_{ap}-E_{corr})$. Because the anodic and cathodic Tafel slopes for these materials in radiolyzed DI water were not known (and not easily determined) they were assumed to be 0.12V/decade current. It may be noted that the minimum and maximum allowable values for $_a$ and $_c$ typically differ only by a factor of 3 (0.06 and 0.18V respectively), therefore, i_{corr} is more sensitive to changes in R_{pol} as compared to $_a$ and $_c$(29). From i_{corr}, the corrosion rate (CR, in 10^{-6} m/yr.) was determined from the well known expression:

$$CR_{\mu m/yr} = \frac{3277 \left(i_{corr} EW\right)}{}$$ (4)

where: i_{corr} is in A/cm^2 x10^{-3}, EW is the equivalent weight in g/equiv., and is density in g/cm^3. Caution is warranted, however, when using Eq. 4 to calculate corrosion rates. As i_{corr} is the

corrosion current density it has been normalized by the total surface area of the sample. Therefore, Eq. 4 yields a surface averaged rate and may not be conservative if pitting type corrosion has occurred. That is, in pitting corrosion the majority of the corrosion current is associated with a very small area on the surface of the sample.

3.3 Corrosion rates in the corrosion loop

Corrosion rates for W and 316L-NG SS are presented in Figures 9 and 10 as a function of immersion time. The irradiation period has been divided into three separate categories in these plots: 1) pre-irradiation, beam off (indicated by negative days), 2) beam on, 0.001-0.40 mA, corrosion insert only (days 0-10), and 3) beam on , 1 mA, all forward inserts in place (after day 10). During experiments when only the corrosion insert was in-beam, the beam spot at the corrosion manifold had a Gaussian distribution of 2 = 3 cm. After day 10, the forward inserts were placed in-beam. This resulted in a decrease in proton flux for any given proton beam current at the corrosion manifold after day 10. As shown in Figure 9 and 10 the corrosion rate of these samples was greatest during the first 10 days of the irradiation period when only the corrosion insert was in place. More importantly, it appears that corrosion rate increased with beam current during this period, the greatest increase being observed in the return side probe. This can be seen more clearly in Figure 11. With only the corrosion loop in place, the corrosion rate of the return side W sample increased from 2.19×10^{-6} m/yr. with the beam off to 3.27×10^{-5} m/yr at a beam current of 0.40 mA. In comparison, the change in corrosion rate of the supply side probe appears to be less dependent on beam current. In addition, the observed changes in W corrosion rate appear to be independent of water resistivity (Figure 12). One would anticipate that corrosion rate would be inversely proportional to water resistivity.

Changes in the corrosion rate of Al6061, and Al5052 (corrosion loop Figure 13 and 14 respectively) appear to be similar for the return and supply side probes and independent of beam current or irradiation time. Although a small "peak" in corrosion rate around day 40 was observed in 3 of the 4 samples. This peak corresponds to a minimum in the water resistivity on day 40. After day 40 a small (unrepairable) leak in the water system (approximately 1 L/hour) required

fresh DI to be pumped into the system to maintain operating conditions. As anticipated, this resulted in an increase in water resistivity in the corrosion loop after day 40 (Figure 12). The highest corrosion rates for the aluminum alloys were observed during the pre-irradiation period. This was attributed to chloride, sulfate, and other contaminants that may not have been removed from the system during the cleaning process. After several flush and refills of the corrosion water system during the pre-irradiation period, initial water resistivity rose to approximately 7.8×10^4 ohm·cm prior to irradiation. The low resistivity in the first several days before the beam was turned on likely owed to impurities that were being washed from the walls of the water system. After turning the proton beam on, a sharp decrease in the water resistivity from 7.8×10^4 to 4.1×10^4 ohm·cm was observed.

Gamma analysis of water samples taken from the corrosion loop found that the water activity owing to Mn^{54}, Co^{56}, Co^{60} increased with proton irradiation time (Table 2). These levels were relatively low, and were attributed to the relatively low corrosion rates of the 304 SS water system as well as the in-beam Alloy 718 corrosion samples. This was confirmed by ion coupled plasma (ICP) measurements which found no measurable iron in the system and only trace levels of Mg, Zn, Cu, and Ca impurities . The concentration of these impurities remained relatively constant during the irradiation period (Table 2). In addition, as similar concentrations of these impurities were found in the unirradiated DI water and, therefore, are not a result of corrosion or other sources of system contamination.

Steady state H_2O_2 formation in the corrosion water loop was measured by iodometric titration of water samples taken from the system (a technique sometimes called Kingzettís method). Briefly, a volume of irradiated water is placed in a conical flask. Enough sulfuric acid was added to the water to adjust the pH to 1 (approximately). An excess amount of iodide ions, I^-, is added to this solution, thereby liberating triiodide ions:

$$H_2O_2 + 3I^- \quad I_3^- + 2H_2O$$
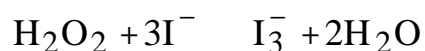
The reaction is quantitative: each hydrogen peroxide molecule reacts and produces exactly one triiodide ion; the excess iodide ions remain in solution and do not interfere with the rest of the analysis. The triiodide ions liberated are then titrated with a standardized solution of sodium thiosulfate. While no H_2O_2 was detected in the corrosion loop during the first 20 days of irradiation, the H_2O_2 concentration gradually increased to a final value of 11.4 ppm. This value was quite low in comparison to the amount of H_2O_2 the system was theoretically capable of producing(4). While this may owe to HWC, H_2O_2 formation may be self limiting as water radiolysis also produces a substantial amount of hydrogen. That is, in the absence of HWC, a sufficient concentration of H may be produced due to radiolysis such that the actual H2O2 concentration is far below the theoretical value.

The corrosion rate of the 304L SS, Alloy 718, and Ta samples (corrosion loop Figures 15-17) were apparently immune to changes in water chemistry, beam current, or irradiation time. No trends in corrosion rate with immersion time were observed in these samples. In addition, the corrosion rates of all of these samples were less than 1.2×10^{-7} m/yr. Although the Ta corrosion rates were the lowest observed (Figure 17), the rate of the supply side Ta sample increased with time independent of the proton beam current or flushing of the water system. Therefore, this trend is likely due to a change in the probe or sample integrity such as crevicing at the Viton gasket or the failure of this gasket to adequately insulate the Ta sample from the probe assembly. Unfortunately, due to the high radiation levels, the necessary visual access to the sample to confirm this was not possible .

3.4 Corrosion rates in the degrader loop

Similar trends in corrosion rate with beam current were observed for materials in the degrader loop. With the beam off, the corrosion rates for Cu in the return and supply side streams were approximately the same, 1.3×10^{-7} and 9.6×10^{-8} m/yr. respectively (Figure 18). Upon turning the proton beam on to a current of 1.0 mA, the corrosion rate of the return side Cu sample increased to 5.7×10^{-7} m/yr. while the corrosion rate of the supply side Cu sample remained the same.

The long-term corrosion rates for Alloy 718, 304L SS, and Al6061 were considerably higher than those measured for these same materials in the corrosion loop (Figure 19). For example, after 40 days of immersion (approximately 10^{20} p/cm^2) the corrosion rates of Al6061 and 304L SS in the corrosion loop were approximately 5.5 x10^{-7} m/yr. and 5.4 x10^{-8} m/yr. respectively. In comparison, the corrosion rates of Al6061 and 304L SS in the degrader loop after 40 days of immersion were approximately 5.6 x10^{-6} m/yr and 1.9x10^{-6} m/yr. This change in corrosion rate is attributed to changes in water quality during irradiation as seen in the return stream water resistivity measurements for the degrader loop. During the irradiation period, water resistivity decreased from its initial value of approximately 1 x10^5 ohm·cm to a final value of 1.7 x10^3 ohm·cm at the end of the irradiation period(Figure 20). This decrease was attributed to an increase in both radiolysis and corrosion products. Recall that the water in the water degrader loop had a resonance time of approximately 16 seconds at the proton beam, thus increasing the quantity of radiolysis that may have occurred. In comparison, water in the corrosion loop manifold was not associated with a resonance time, therefore, radiolysis production was likely lower in the corrosion loop. Post irradiation analysis of the degrader loop water system found that copious amounts of Cu^{++} (in the form of Cu/CuO) that had plated out on virtually all components. Copper precipitation was not an issue in the corrosion water loop system as it was entirely fabricated of 304 SS and contained no Cu corrosion samples. It has been recognized for quite some time that Cu/CuO precipitation increases cathodic reaction rates and thus metal corrosion(6). Although this phenomena occurs in nickel and iron base alloys, aluminum alloys are particularly sensitive to Cu precipitation which likely explains the relatively high rates of aluminum corrosion observed in the degrader loop (Figure 19).

4. Conclusions

A method for measuring the real-time corrosion rates of materials in water irradiated by 800 MeV protons has been presented. The effects of water system fabrication materials, hydrogen water chemistry, and pre-cleaning of the water system on corrosion rate have been demonstrated to be dramatic. In the corrosion loop which was fabricated entirely of 304 SS, thoroughly cleaned before operation, and employed hydrogen water chemistry to mitigate the formation of radiolysis products, the corrosion rates for stainless steels, Alloy 718, and tantalum were extremely low, less than 1.2×10^{-7} m/yr. For Al6061 and Al5052 the corrosion rates were slightly higher than the iron and nickel base alloys, on the order of 5.0×10^{-7} to 2.0×10^{-6} m/yr. The corrosion rate of tungsten was found to be (relatively) high, between 5.0×10^{-6} and 3.0×10^{-5} m/yr. In comparison, the corrosion rates of these materials in the degrader water loop which was fabricated from copper piping and stainless steel, was not cleaned prior to operation, and employed no HWC the corrosion rates were 1-3 orders of magnitude higher.

Theses results were attributed to a change in water purity and a build up of water radiolysis products within the closed loop systems. In the system with the lowest corrosion rates (corrosion loop) the water resistivity remained between approximately 8×10^{4} to 3×10^{4} ohm·cm. The largest decrease in resistivity was observed when the proton beam was turned on. In comparison, during the same time period, the resistivity of degrader water loop fell from its initial value of approximately 1×10^{5} ohm·cm to 2×10^{3} ohm·cm. ICP analysis, iodometric titration, and Gamma analysis of the water from the corrosion loop were consistent with resistivity measurements. ICP analysis of water samples found only trace amounts of Mg, Zn, Cu, and Ca, believed to come from the DI water as they were observed prior to turning the beam on and their concentration was independent of irradiation time. Iodometric titration of water samples found that the concentration of H_2O_2 in the water system at the end of the irradiation period was lower than anticipated, 11.4 ppm. In comparison, post irradiation analysis of the degrader loop water system found that copious amounts of Cu^{++} (in the form of Cu/CuO) that had plated out on virtually all of the components.

15

Acknowledgments

References

[1]   T. K. Yeh, D. D. MacDonald, A. T. Motta, Nuclear Science and Engineering, 121 (1995) 468.

[2]   H. Christensen, Nuclear Technology, 109 (1994) 373.

[3]   J. L. Magee, A. Chatterjee, in: Kinetics of Nonhomogeneous Processes, G. R. Freeman (Ed), John Wiley & Sons, New York, 1987, p. 171.

[4]   L. L. Daemen, et al., in Materials for Spallation Neutron Sources, M. S. Wechsler, L. K. Mansur, C. L. Snead, W. F. Sommer (Eds), Orlando, FL, February 10-12,1997, TMS, Warrendale, PA, 1998.

[5]   W. G. Burns, P. B. Moore, Radiation Effects, 30 (1976) 233.

[6]   H. Kaesche, Metallic Corrosion, NACE, 1985.

[7]   M. E. Indig, J. E. Weber, in: Corrosion/83, NACE, Houston, TX, 1983, paper no. 124.

[8]   W. R. Kassen, R. P. Jones, J. L. Tollefson, in: Corrosion/92, NACE, Houston, TX, 1992, paper no. 112.

[9]   M. Fox, in: Corrosion/83, NACE, Houston, TX, 1983, paper no. 123.

[10]   C. C. Lin, R. L. Cowan, R. S. Pathania, in: Corrosion/93, NACE, Houston, TX, 1993, paper no. 619.

[11]   L. G. Ljungberg, D. Cubicciotti, M. Trolle, in: Corrosion/85, NACE, Houston, TX, 1985, paper no. 100.

[12]   M. J. Fox, A Review of Boiling Water Reactor Chemistry: Science, Technology, and Performance, Argonne National Laboratory for the US Nuclear Regulatory Commision NUREG/CR-5115 ANL-88-42 (1989).

[13]   Y. J. Kim, in: Corrosion/96, NACE, Houston, TX, 1996, paper no. 102.

[14]   Y. J. Kim, P. L. Andresen, T. M. Angeliu, in: Corrosion/96, NACE, Houston, 1996, paper no. 109.

[15]   R. S. Glass, G. E. Overturf, R. A. V. Konynenburg, R. D. McCright, Corrosion Science, 26 (1986) 577.

[16]   Y. J. Kim, R. A. Oriani, Corrosion, 43 (2) (1987) 92.

[17]   A. V. Byalobzheskii, Radiation Corrosion (Russion translation), Keter Press, Jerusalem, Isreal, 1970.

[18]   S. Fujimoto, T. Yamada, T. Shibata, Journal of the Electrochemical Society, 145 (1998) L79.

[19]   Y. J. Kim, R. A. Oriani, Corrosion, 43 (1987) 85.

[20]   G. Capobianco, G. Palma, G. Granozzi, A. Glisenti, Corrosion Science, 33 (1992) 729.

[21]   R. S. Lillard, D. P. Butt, accepted for publication in: Materials Characterization, (1999) .

[22]   R. S. Lillard, D. P. Butt, Journal of Materials, Dec (1998) 56.

[23]   R. S. Lillard, D. L. Pile, D. P. Butt, submitted to: The Journal of Nuclear Materials, (1999) .

[24]   W. F. Sommer, APT Materials Safety Experiments Technical Report, Los Alamos National Laboratory LAUR-93-2850 (1993).

[25]   L. B. Kriksunov, D. D. MacDonald, P. J. Millet, Journal of the Electrochemical Society, 141 (1994) 3002.

[26]   I. Epelboin, C. Gabrielli, M. Keddam, H. Takenouti, in: Electrochemical Corrosion Testing, ASTM STP 727, F. Mansfeld, U. Bertocci (Eds), ASTM, Philadelphia, 1981, p. 150.

[27]   D. D. MacDonald, in: Electrochemical Corrosion Testing, ASTM STP 727, F. Mansfeld, U. Bertocci (Eds), ASTM, Philadelphia, 1981, p. 110.

[28]   J. O. M. Bockris, A. K. N. Ready, Modern Electrochemistry, Volume 2, Plenum Publishing Corp., New York, 1973.

[29]   F. Mansfeld, in: Electrochemical Techniques, R. Baboian (Ed), Nace, Houston, 1986, p. 67.

Table 1 Elementary equations showing some of the water radiolysis products formed during irradiation, their decomposition mechanism, rate constant, and activation energy (from ref.**5**).

Reaction	Rate Constant $(sec)^{-1}$	Activation Energy (J/mol)
$e^- + H_2O = H + OH^-$	2.4×10^{10}	1.26×10^4
$e^- + OH = OH^-$	3.0×10^{10}	1.26×10^4
$H + H = H_2$	1×10^{10}	1.26×10^4
$e^- + HO_2 = HO_2^-$	2×10^{10}	1.26×10^4
$OH + OH = H_2O_2$	**4.5×10^9**	**1.26×10^4**
$H + OH = H_2O$	**2.4×10^{10}**	**1.26×10^4**
$H + O_2 = HO_2$	1×10^9	1.26×10^4
$OH^- + H_2O_2 = HO_2^- + H_2O$	1×10^8	1.26×10^4
$HO_2 = O_2^- + H^+$	8×10^5	1.26×10^4

Table 2 Gamma and ICP analysis of water samples taken from the corrosion water loop as a function of time. Hydrogen peroxide concentration from iodometric titration is also presented. The beam was turned on at day 0, therefore, negative days indicate the period before the beam was turned on. The abbreviation **nd** stands for none-detected.

days of beam	Gamma analysis (dpm)							ICP Analysis (ppm)				
	Be^7	Mn^{54}	Sc^{64}	Co^{56}	Co^{60}	W	Mg	Zn	Cu	Ca	Fe
-11	nd	nd	nd	nd	nd	0.01	0.03	0.04	0.02	2.6	nd
	flush / refill system after day -6										
7	$2.3\ 10^4$	100	nd	nd	nd	nd	0.13	0.45	0.04	2.9	nd
	flush / refill system after day 7										
9	$8.7\ 10^4$	400	178	nd	nd	0.06	0.05	0.19	0.04	1.9	nd
66	$4.0\ 10^6$	$9.2\ 10^3$	465	$7.4\ 10^3$	840	0.63	0.09	0.30	0.03	2.4	nd
132	H_2O_2 concentration = 11.4 ppm										
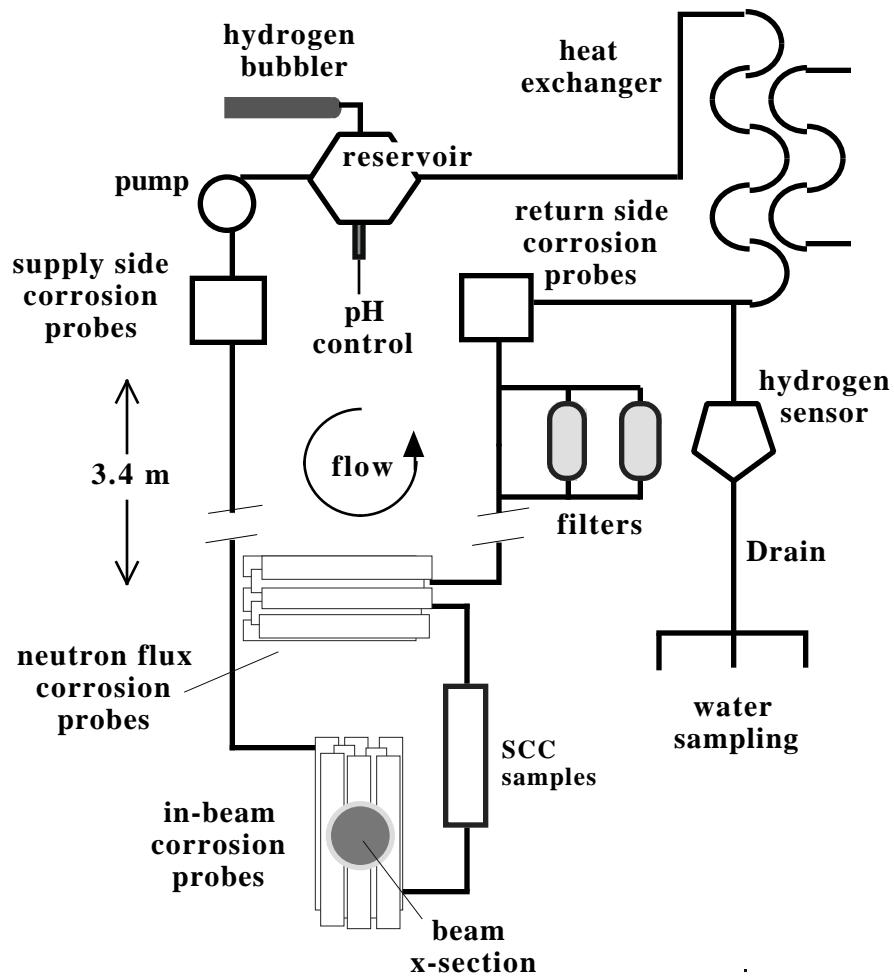
Figure 1a Diagram representing the corrosion water loop system. The 800 MeV proton beam struck the water loop at the base of the insert (in-beam corrosion probes). The radiolyzed water then circulated from the beam spot through the remainder of the loop including the out-of-beam probes.
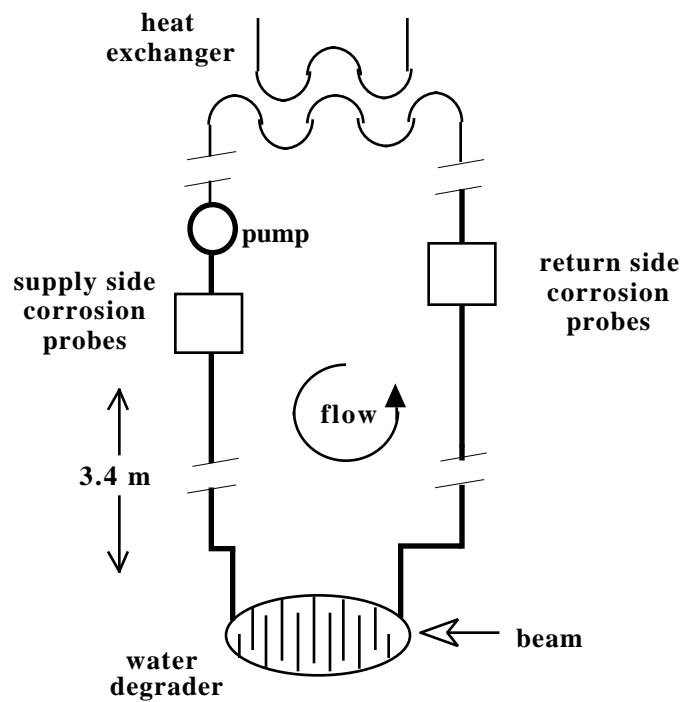
Figure 1b   Diagram representing the water degrader system. Water circulated through the degrader where it was irradiated by 800 MeV protons. The radiolyzed water then circulated from the beam spot through the remainder of the loop including the out-of-beam probes.
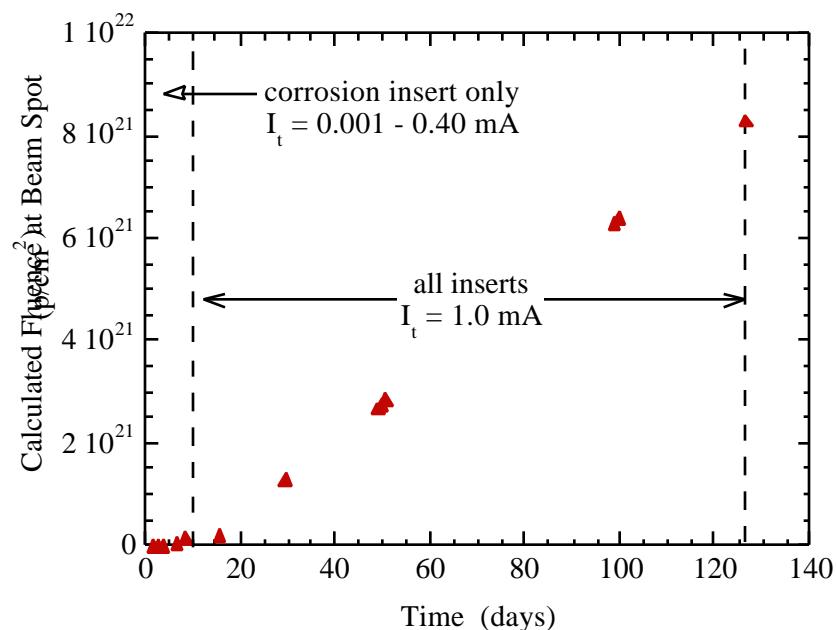
Figure 2 Calculated proton fluence at the corrosion loop manifold as a function of irradiation time (in accordance with ref **23**). I_t represents the proton beam current.
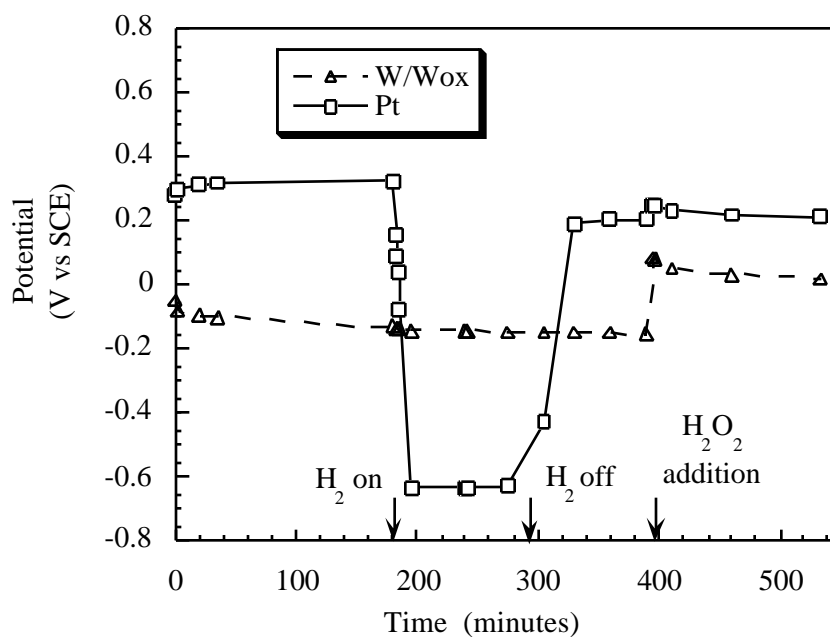
Figure 3 OCP of the tungsten / tungsten-oxide and platinum electrodes (vs. saturated calomel electrode SCE) as a function of time. Plot shows the effect of bubbling H_2 gas into solution and the addition of 0.1 M H_2O_2 on the OCP of these electrodes.
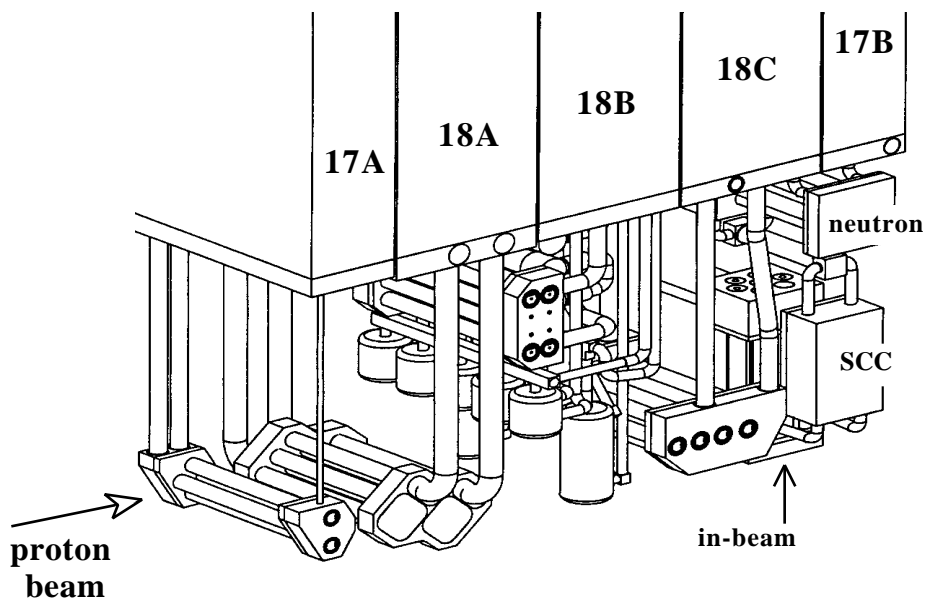
Figure 4 A diagram representing the A6 Target Station at LANSCE and placement of the corrosion loop (17B). Early in-beam data reported on for the corrosion loop were collected with inserts 17A-18C removed from the beam path. At later times, inserts 17A-18C were placed in-beam as shown in this figure.
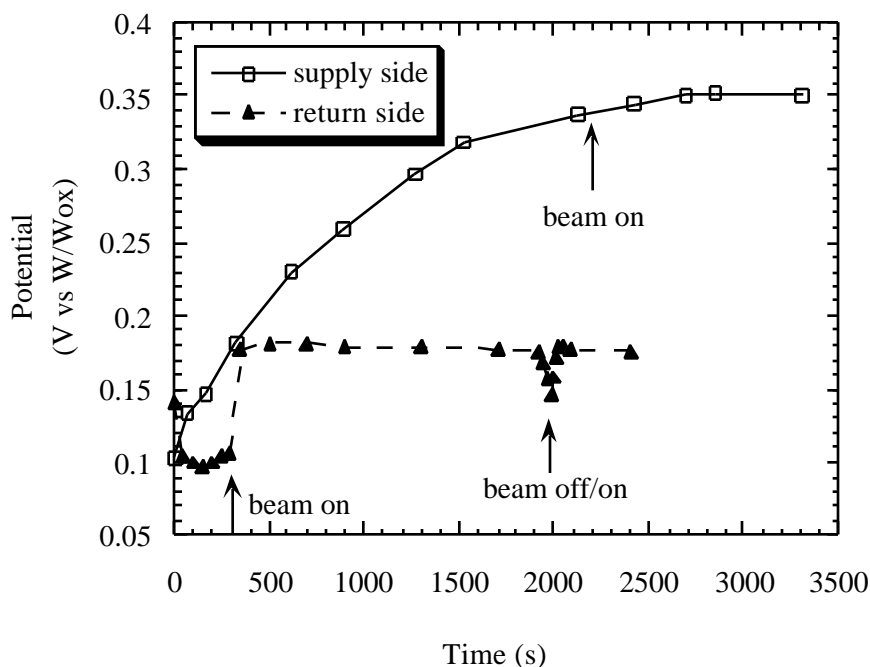
Figure 5 OCP of the return and supply side Cu samples in the water degrader loop. Although plotted on the same graph, the return and supply experiments were conducted at different times, that is, 'beam on' during the return side experiments does not correlated with beam on in the supply side experiment.
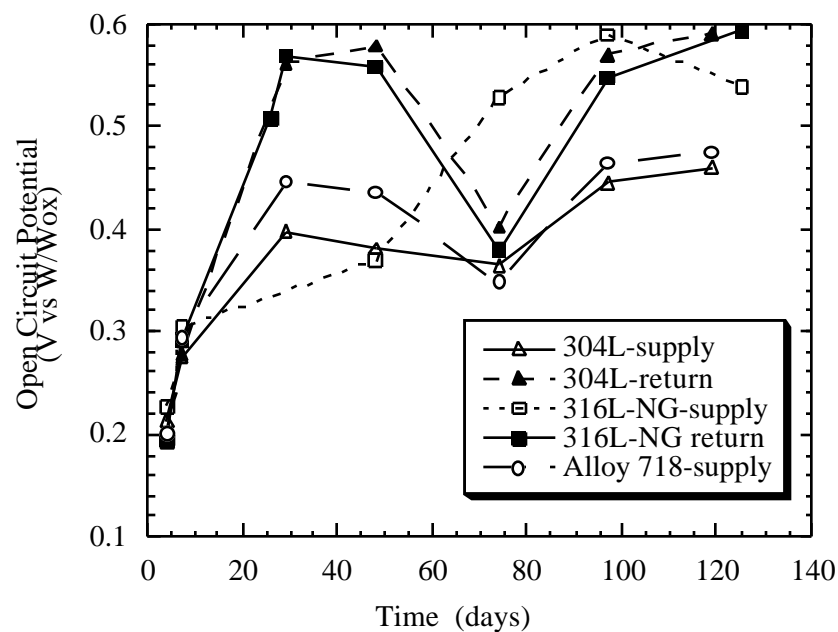
Figure 5 OCP of 304L SS, 316L-NG SS, and Alloy 718 samples in the corrosion water loop for both the supply side, and return side as a function of irradiation time.
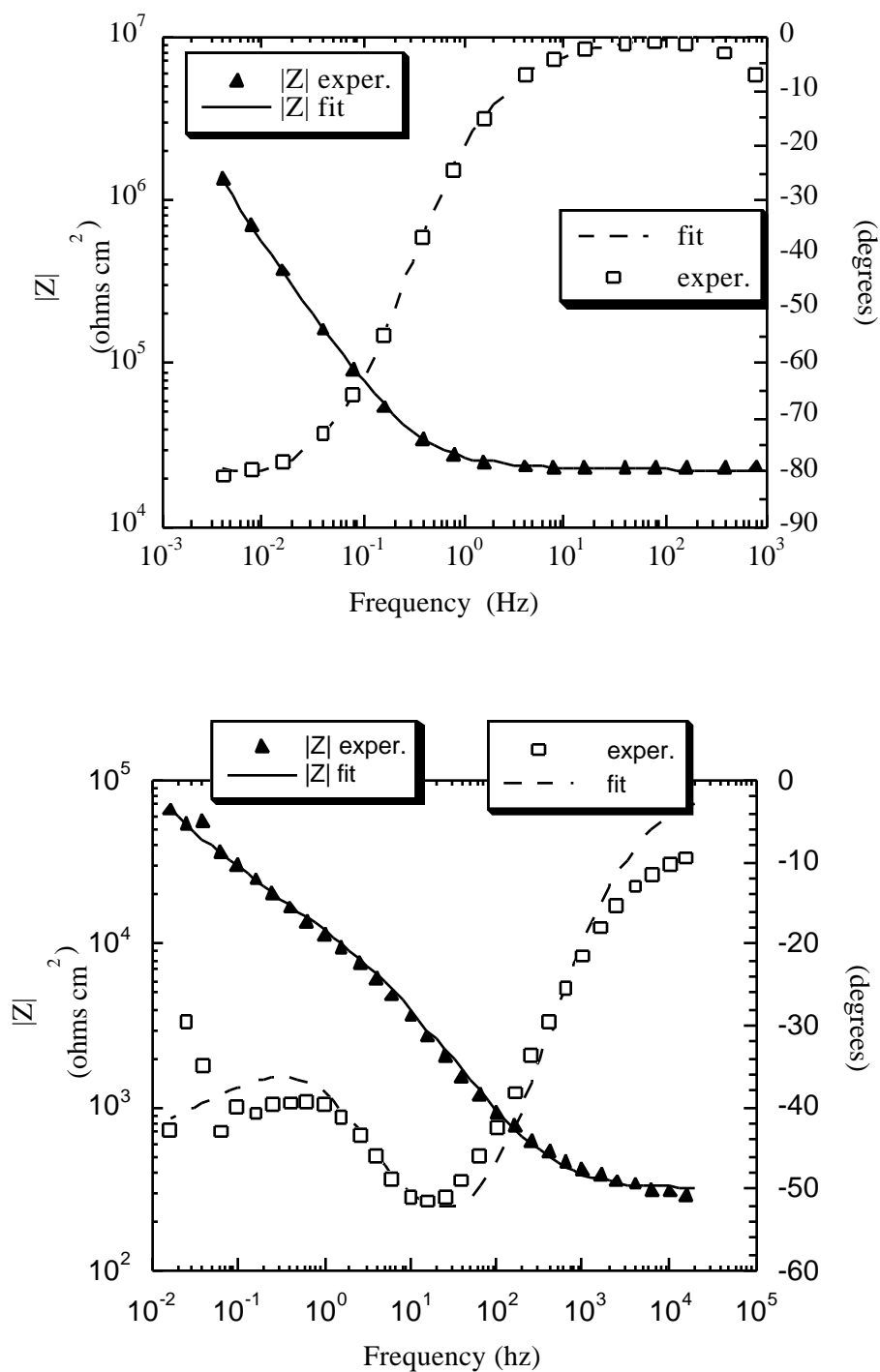
Figure 5 Bode magnitude |Z| and phase ( ) plots for the out-of-beam **a-top)** Alloy 718 sample (supply side, corrosion loop) and **b-bottom)** 304L SS sample (return side, water degrader loop). Not all experimental data (□/▲) is presented. Solid and dashed lines represent complex non-linear least square fits to the data.
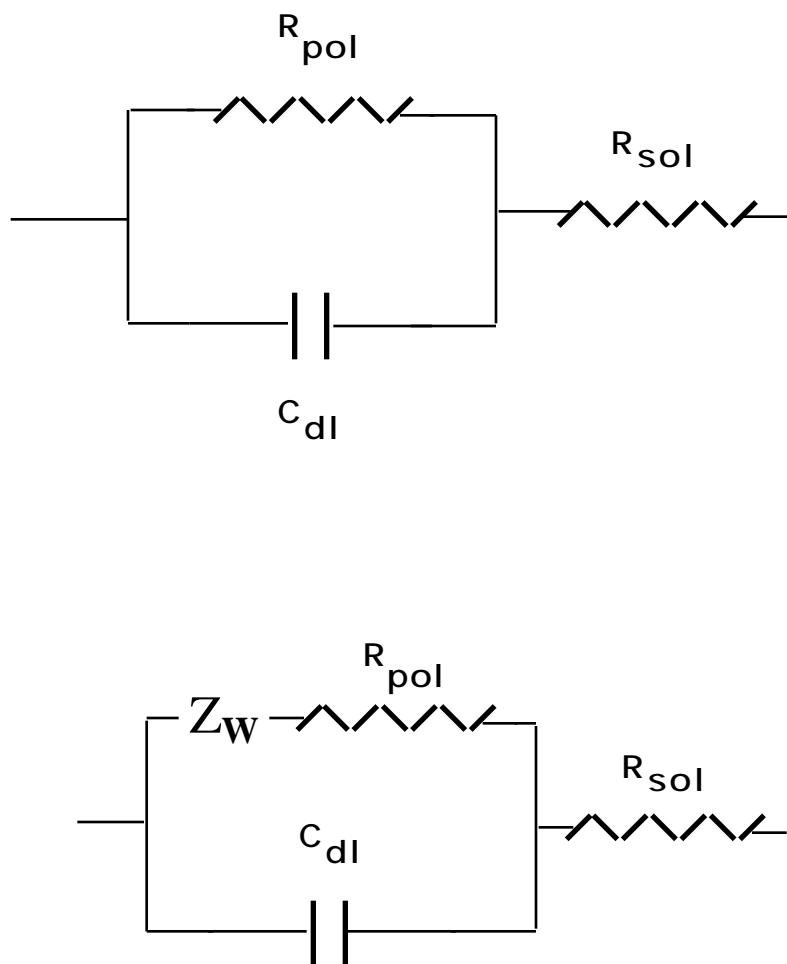
Figure 6 Electrical equivalent circuits used to model EIS data: **a-top)** simplified Randle's circuit and **b-bottom)** diffusion impedance circuit.
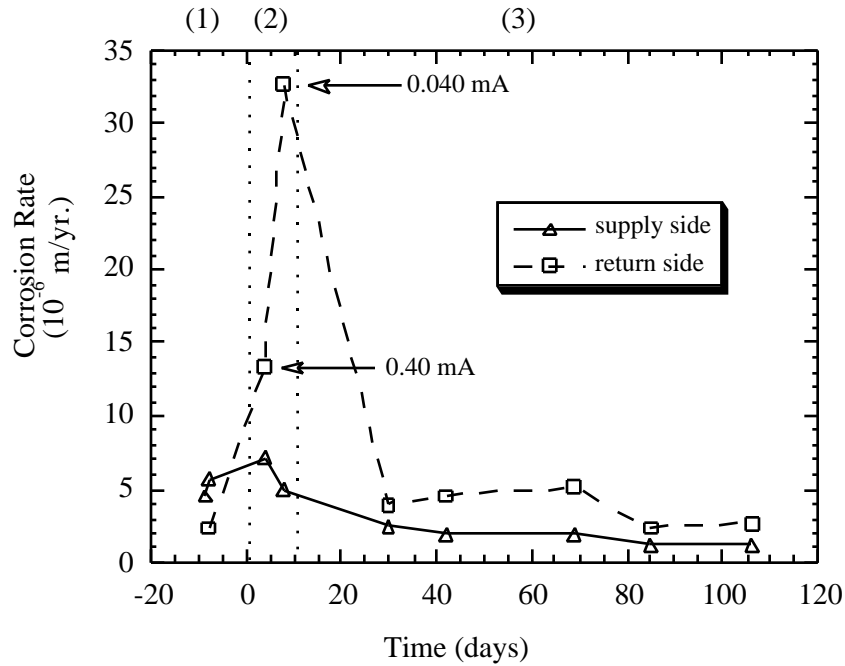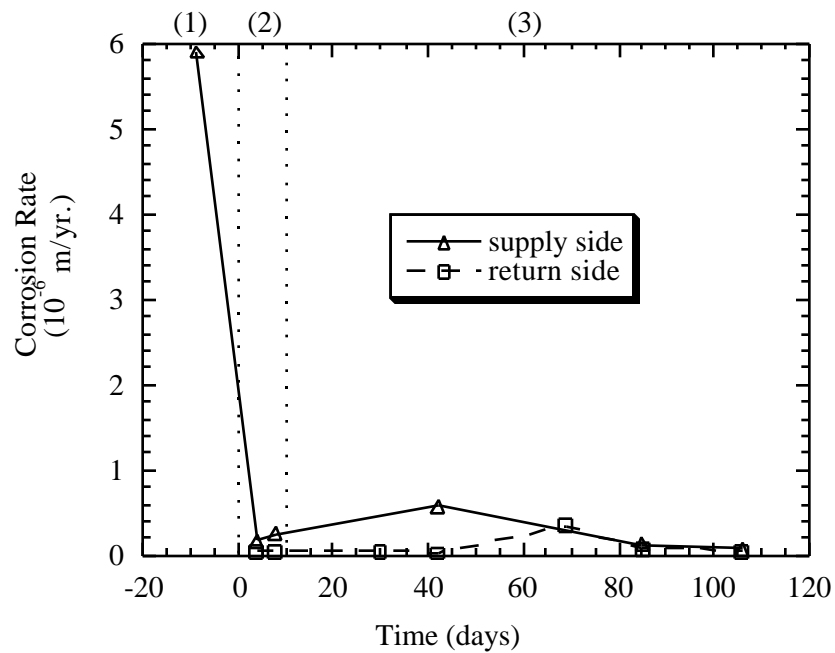
Figure 9 Corrosion rates for W in the corrosion water loop as a function of irradiation time. The irradiation period has been divided into three separate categories: 1) pre-irradiation, beam off, 2) beam on, 0.001-0.40 mA, corrosion insert only, and 3) beam on, 1 mA, inserts 17A-18C in place.
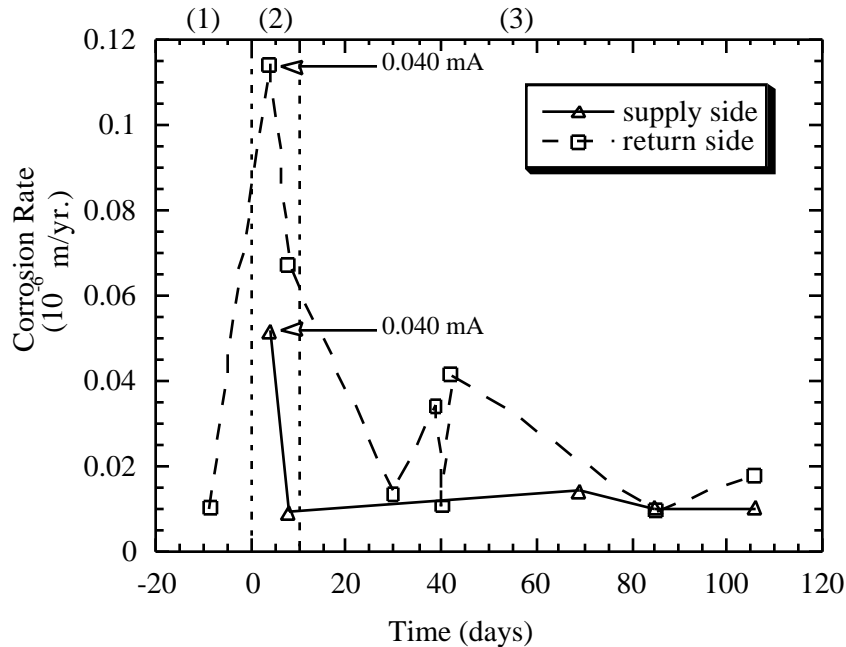
Figure 10 Corrosion rates for 316L-NG SS in the corrosion water loop as a function of irradiation time. The irradiation period has been divided into three separate categories as described in Figure 2 and Figure 8.
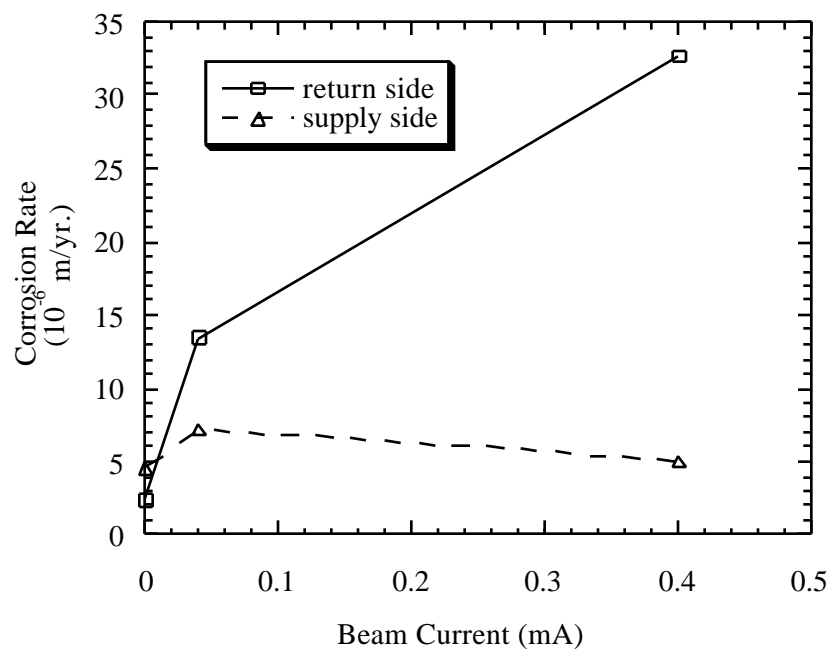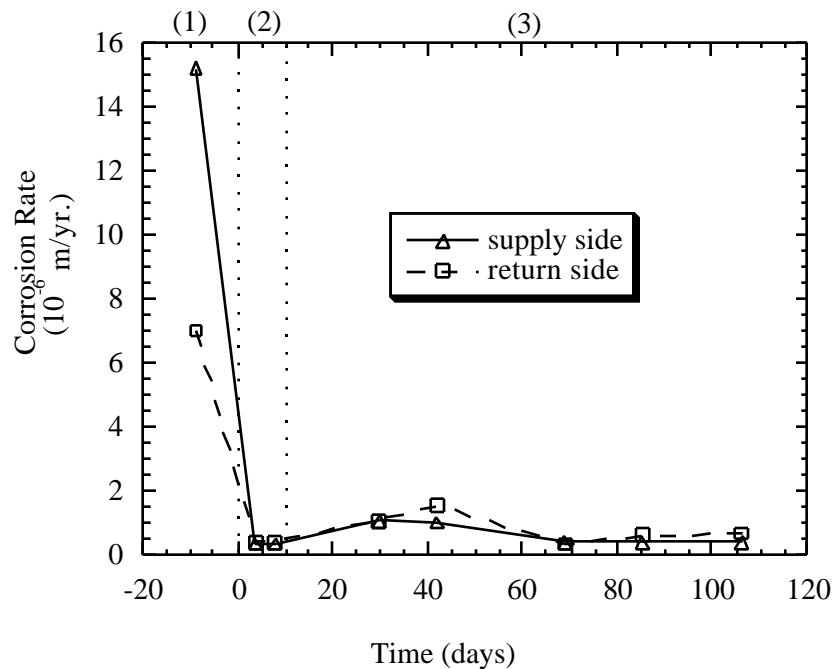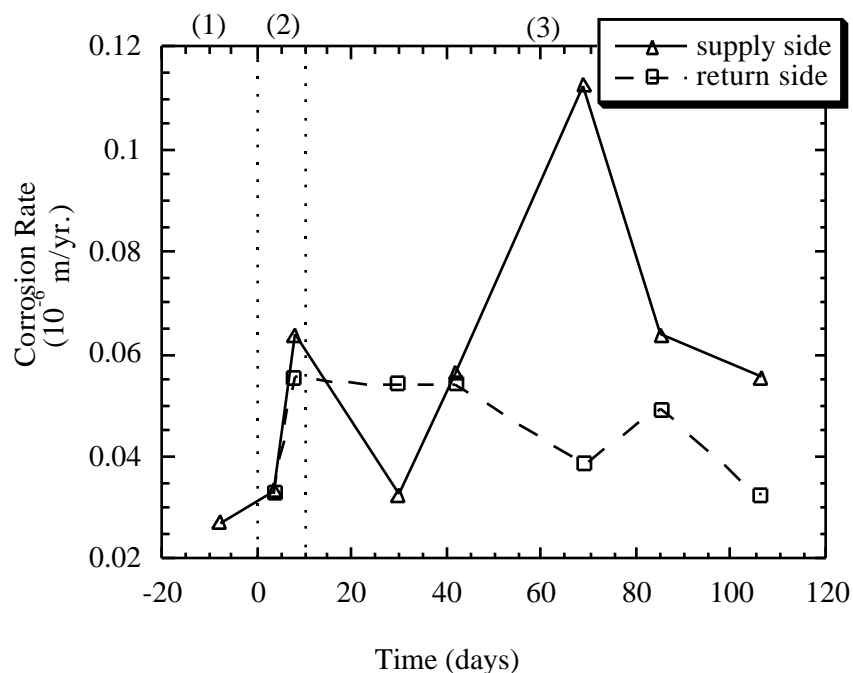
Figure 11 Corrosion rates for W in the corrosion loop as a function of beam current. Data taken during days 0-10, corrosion insert only (section (2) in Figure 9).
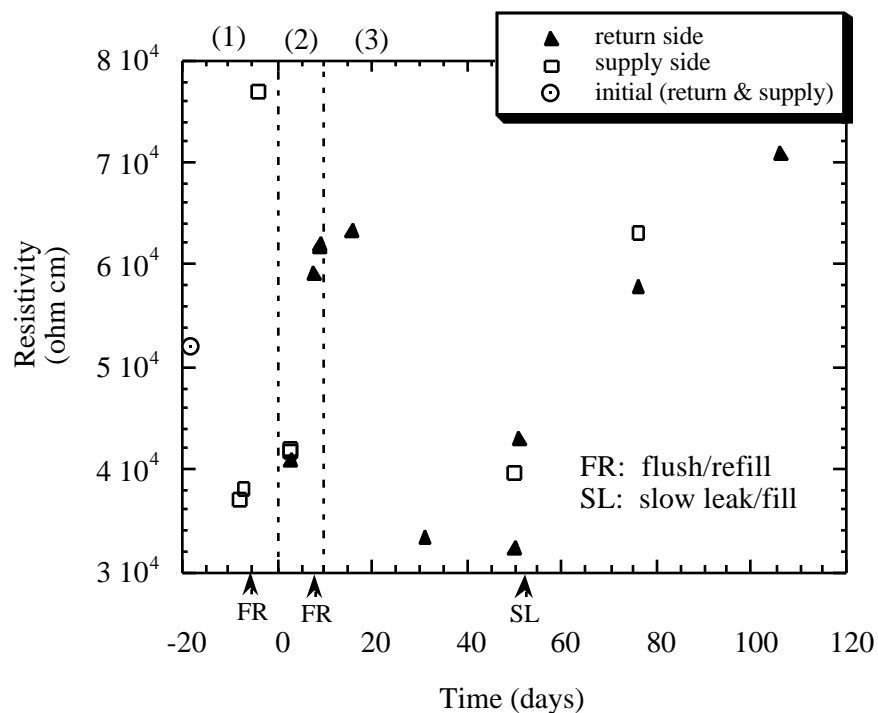
Figure 12 Water resistivity from the corrosion loop as a function of irradiation time as measured by the supply and return probes. The irradiation period has been divided into three separate categories: as presented in Figure 2 and Figure 8.

29

Figure 13 Corrosion rates for Al6061 in the corrosion water loop as a function of irradiation time. The irradiation period has been divided into three separate categories as described in Figure 2 and Figure 8.
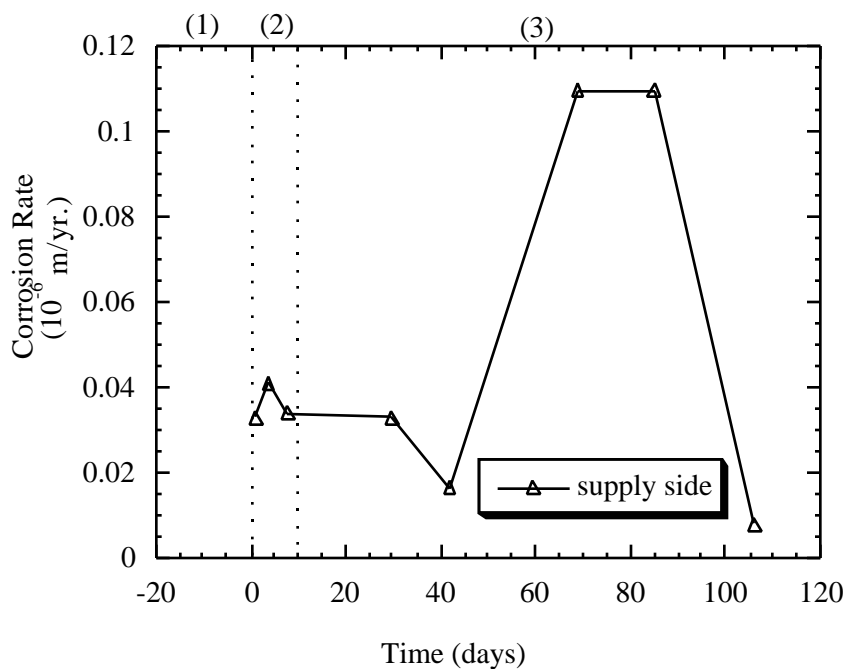

Figure 14 Corrosion rates for Al5052 in the corrosion water loop as a function of irradiation time. The irradiation period has been divided into three separate categories as described in Figure 2 and Figure 8.
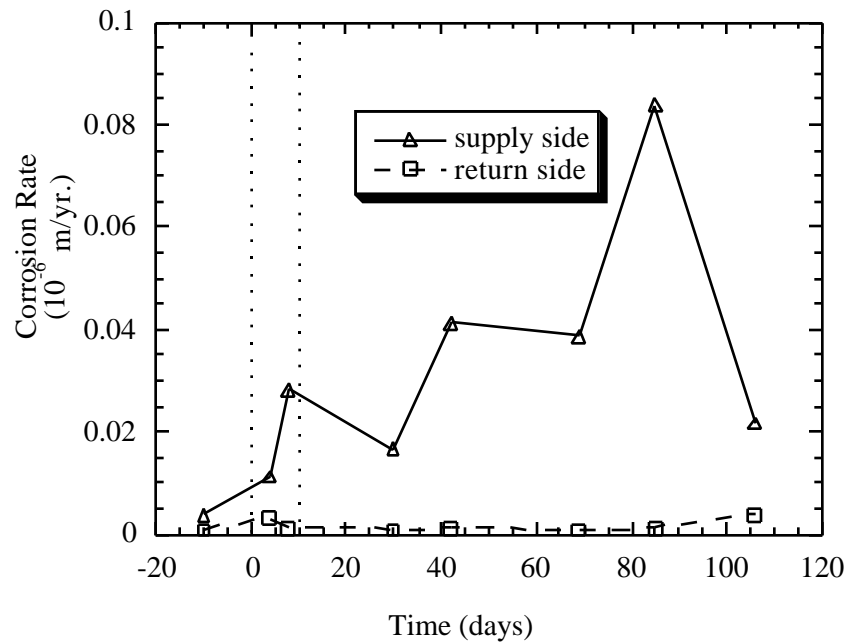
Figure 15   Corrosion rates for 304L SS in the corrosion water loop as a function of irradiation time. The irradiation period has been divided into three separate categories as described in Figure 2 and Figure 8.

Figure 16   Corrosion rates for Alloy 718 in the corrosion water loop as a function of irradiation time. The irradiation period has been divided into three separate categories as described in Figure 2 and Figure 8.
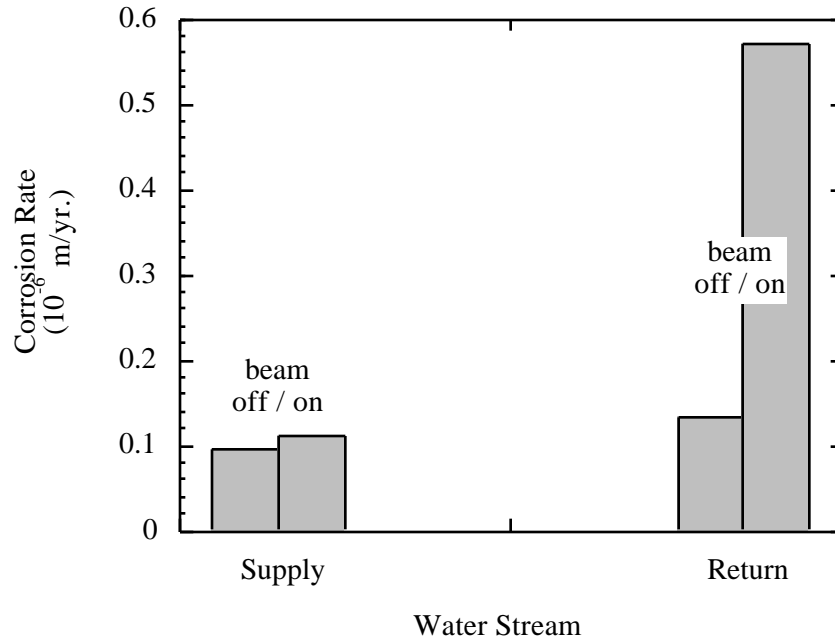
Figure 17 Corrosion rates for Ta in the corrosion water loop as a function of irradiation time. The irradiation period has been divided into three separate categories as described in Figure 2 and Figure 8.

Figure 18 Corrosion rates for Cu from the degrader loop. data were taken on day 0 in Figure 19 before and after the proton beam was turned on at 1.0 mA.
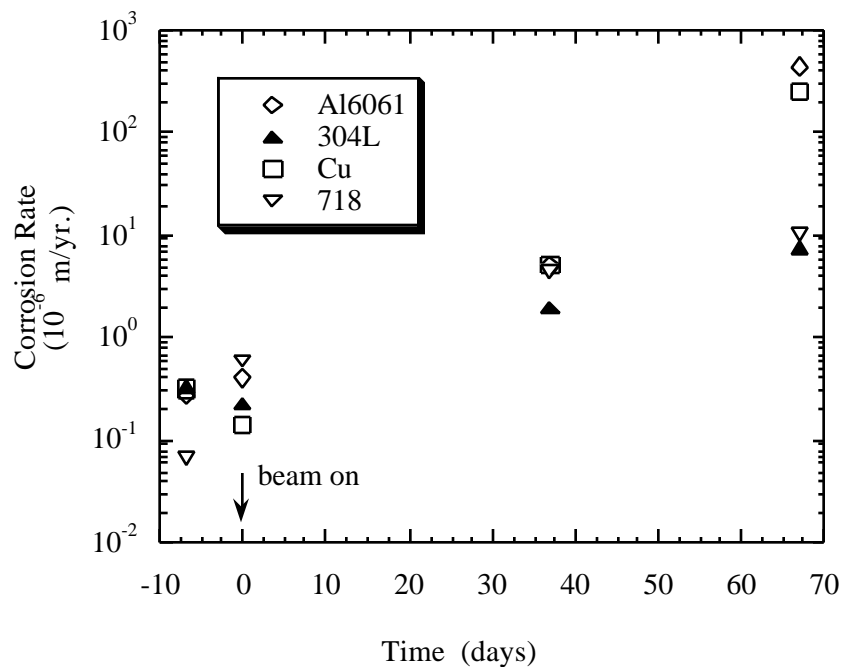
Figure 19 Corrosion rate for Al6061, 304L SS, Cu, and Alloy 718 in the degrader water loop (return side) as a function irradiation time. Negative time indicates the pre-irradiation period (beam off). Proton beam current was 1.0 mA throughout the irradiation period.
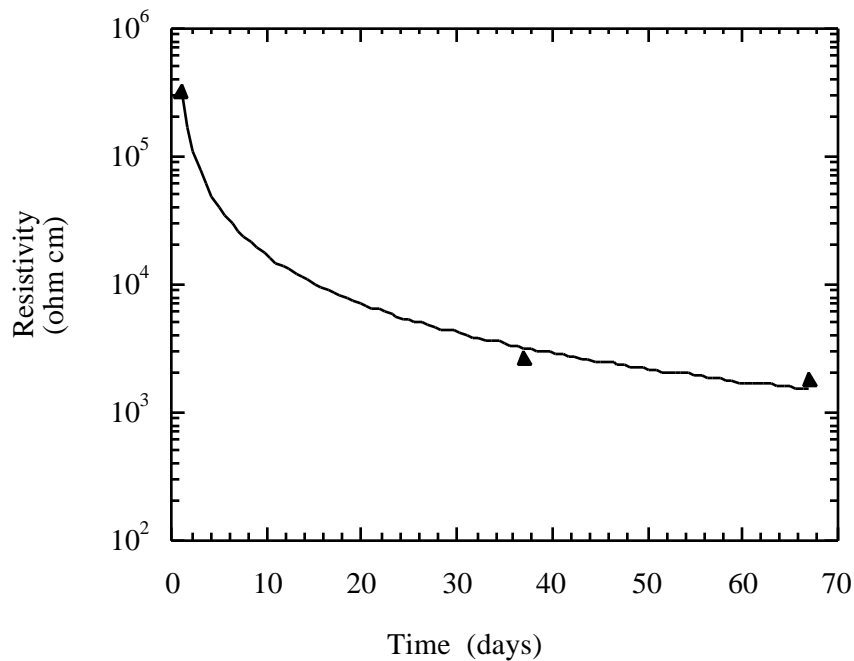

Figure 20 Water resistivity from the degrader loop as a function of irradiation time (return stream only).